

High Power Characterization of Piezoelectric Materials Using the Burst/Transient Method with Resonance and Antiresonance Analysis

Husain Shekhani^{1*}, Timo Scholehwar², Eberhard Hennig², and Kenji Uchino¹

¹Department of Electrical Engineering, The Pennsylvania State University, University Park, Pennsylvania, 16801, USA

²PI Ceramic GmbH, Lederhose, 07589, Germany

Abstract

In this paper, a comprehensive methodology for characterizing the high power resonance behavior of bulk piezoelectric ceramics using the burst method is described. In the burst method, the sample is electrically driven at its resonance frequency, and then either a short circuit or an open circuit condition is imposed, after which the vibration decays at the resonance or antiresonance frequency, respectively. This decay can be used to measure the quality factor in either of these conditions. The resulting current in the short circuit vibration condition is related to the vibration velocity through the “force factor.” The generated voltage in the open circuit vibration condition corresponds to the displacement by the “voltage factor.” The force factor and the voltage factor are related to material properties and physical dimensions of the sample. Using this method, the high power behavior of the permittivity, compliance, piezoelectric charge constant, electromechanical coupling factor, and material losses can be determined directly by measuring the resonance (short circuit) and antiresonance (open circuit) frequencies, their corresponding quality factors, the force factor A , and the voltage factor B . The experimental procedure to apply this method is described and demonstrated on commercially available hard and semi-hard PZT materials of k_{31} geometry.

1 Introduction

Piezoelectric materials are used in a variety of high power applications such as ultrasonic motors and underwater sonar transducers. The properties of these materials are subject to the conditions in which they are applied in.

* Author to whom correspondence should be addressed. Electronic mail: hns116@psu.edu

Therefore, the properties must be measured in comparable high power testing environments in order to achieve relevant measurements. This paper uses the burst/transient method for measuring the properties of piezoelectric materials in high power conditions using a comprehensive approach with resonance and antiresonance analysis. The burst method offers several advantages over other high power measurement methods: appropriate application of linear theory, short measurement time, data collection over large range of vibration levels in single measurement, simplicity in experimental application, and no heat generation/temperature rise during measurement.

Two methods are commonly used to determine the material properties in piezoelectric ceramics in high power resonance conditions: resonance electrical spectroscopy and the burst/transient method. In resonance impedance spectroscopy, the sample is continuously driven electrically, and its electrical impedance or admittance is measured across its resonance and antiresonance frequency. By fitting an equivalent circuit or by utilizing a power bandwidth approach, the loss factors and material properties for a particular vibration mode can be calculated. Using the resonance frequency, the elastic compliance can be measured. Utilizing the relative difference between the resonance and antiresonance frequencies, the electromechanical coupling factor can be calculated. [1, 2]

The second method of measuring properties in high power conditions is through the burst or transient method. In this method, the ceramic is driven using a large excitation voltage at its resonance frequency for a set number of cycles. Then, a short circuit condition is imposed and the sample's oscillation rings down at its resonance frequency. In this case, the short circuit current is proportional to the vibration amplitude. If instead, an open circuit condition is imposed, the sample's oscillation rings down at its antiresonance frequency. In this case, the open circuit voltage is proportional to the displacement. By measuring the rate of signal decay, the loss factors at resonance and antiresonance can be calculated using an incremental time constant formulation. Using the resonance and antiresonance frequencies, the elastic compliance and electromechanical coupling factor can be calculated similarly to the process of the impedance method. The burst method can be considered as a mechanical excitation method because electrical stimulation is not applied during the measurement period. [1, 3, 4].

In the burst/transient method experiment, temperature rise is not generated due to low driving times (often less than 10ms). Also, data for a wide range of vibration levels can be obtained from the decaying oscillation, whereas data must be collected for a single vibration level at a time using the continuous drive method. It has been shown that results from the burst method show higher quality factors (lower losses), and that this is not completely due to temperature rise difference [1, 4]. However, to the authors' knowledge, a rigorous comparison of these techniques has not been made accounting for temperature distribution in the ceramic and number drive cycles. This may lead to comparable results between the two methods.

The burst method was developed by Umeda et al. for determining the equivalent circuit parameters of a piezoelectric transducer [3]. It was thereafter adapted to measure the properties of piezoelectric ceramic samples [4, 5]. The analysis has proved useful to many researchers studying the change of properties with vibration velocity and also to compare property values between materials, especially between PZT and lead-free materials

[6, 7, 8, 9, 10]. However, almost all the analyses have been done at the resonance condition (short circuit). Chang and coworkers have characterized the response of a Langevin Transducer at antiresonance by introducing an open circuit condition to evaluate the equivalent circuit [11, 12, 13]. Also, the open circuit/antiresonance condition has been applied to a hard k_{31} PZT material to characterize its antiresonance quality factor [1, 14]. However, the analytical formulation to derive material properties from the voltage factor and the method to analyze the dielectric permittivity from it will be discussed in this paper for the first time.

The objective of this paper is to provide a comprehensive characterization approach for the k_{31} resonator using the burst method. Some of the techniques have already been presented by previous researchers, but this work adds new analytical methods, supporting experimental techniques, and discussion of physical significance of the high power measurement results.

Firstly, the derivation of the force factor A_{31} and voltage factor B_{31} in terms of material properties and sample geometry will be derived from the constitutive equations for the k_{31} piezoelectric sample. The force factor A_{31} is the relationship between current and vibration in resonance and it is related to the effective piezoelectric stress coefficient e_{31}^* . The force factor analysis for the k_{31} has been presented previously by Takahashi [4], but its explicit derivation has not. The voltage factor B_{31} is the relationship between open circuit voltage and displacement in resonance, related with the effective piezoelectric stiffness coefficient h_{31}^* . We believe it has not been applied nor analyzed in bulk piezoceramics in resonance conditions. Additionally, use of the resonance-antiresonance frequency separation to calculate the electromechanical coupling factor using the burst method will be presented for the first time. Also, the theory for measuring the permittivity directly in resonance conditions will be outlined and demonstrated.

Secondly, the experimental results of the high power resonance response of a hard PZT and semi-hard PZT material of k_{31} geometry will be discussed. The quality factors and the various properties will be measured using application of resonance and antiresonance. The experimental methods to apply the burst method will be described, along with supporting data analysis techniques.

2 Derivation of the force factor and the voltage factor for k_{31} resonators

In this section, the force factor and the voltage factor for the k_{31} resonator will be developed and the approach for calculating material properties will be summarized. Also, the method to characterize the dielectric permittivity in resonance conditions will be described. Fig. 1 shows the geometry of the sample and Tab. 1 defines the symbols used in the derivation as they will appear. The derivations assume a rectangular plate with $a \ll b \ll L$, fully electroded, and poled along the thickness (a). Therefore, the criteria for a k_{31} piezoelectric resonator are met.

The relationship between current and vibration in a resonating piezoelectric ceramic under short circuit and open circuit conditions will be derived for the k_{31} mode. These relationships will be used to experimentally eval-

uate the behavior of piezoelectric samples tested using the burst method in the next section. For the discussion in this paper, the resonance frequency ω_A will be described as A-type resonance and antiresonance frequency ω_B will be described as B-type resonance. The k_{31} mode undergoes mechanical resonance during electrical resonance, corresponding to s_{11}^E . This mode undergoes an electromechanical coupling resonance at its antiresonance frequency, effectively electrically coupling the motional and damped branch of the resonator (Fig. 2) [15]. Electrical antiresonance is achieved by an open circuit (D constant) condition and electrical resonance is achieved by a short circuit condition (E constant).

As long as the sample is symmetric, both in its geometry and boundary conditions, the mode shape will be symmetric about the center of the sample. In general, the mode shape of a piezoelectric resonator with stress free boundary conditions, undergoing vibration in one dimension, with losses, and having finite displacement can be described as

$$u(x, t) = u_0 f(x) \sin(\omega t), \quad (1)$$

where $f(x)$ is a function symmetric about the origin normalized to the displacement at the ends of the piezoelectric resonator, where $f(0) = 0$. Strain is defined as

$$\partial u / \partial x = u_0 f'(x). \quad (2)$$

Then, according to the fundamental theorem of calculus

$$\int_{-L/2}^{L/2} \frac{\partial u}{\partial x} dx = u(L/2, t) - u(-L/2, t) = 2u_0 \sin(\omega t). \quad (3)$$

In general, the vibration or displacement distribution (mode shape) for a k_{31} resonator and the k_{33} resonator is sinusoidal. In general, its mode shape as a function of frequency and normalized to the edge displacement is : for the k_{31} mode [15]

$$u(x) = u_0 \frac{\sin \Omega_{31} x}{\sin \Omega_{31} L/2}. \quad (4)$$

where $\Omega_{31} = \omega / \nu_{11}^E$ and ν is the speed of sound in the material $\nu_{11}^E = 1 / \sqrt{\rho s_{11}^E}$. These mode shape functions define the displacement distribution at resonance modes (e.g. 1st, 2nd, and 3rd mode) and also at frequencies in between. The normalized mode shapes at the first three mechanical resonance modes of the k_{33} and k_{31} resonators are given in Fig. 3. The displacement distribution of frequencies in between resonance modes have distributions of partial wavelengths, unlike mechanical resonance modes, whose distributions of wavelengths of $\frac{1}{2} + (n - 1)$ of the geometry in the direction of vibration.

According to Eq. (3), Eqs. (4) can be written as

$$\int_{-L/2}^{L/2} \frac{\partial \left(u_0 \frac{\sin \Omega_{31} x}{\sin \Omega_{31} L/2} \right)}{\partial x} dx = 2u_0. \quad (5)$$

Eq. (5) does not assume a particular frequency, so the results are true at the mechanical resonance frequency and at other frequencies. Depending on the mode type, either the electrical antiresonance frequency or electrical resonance frequency is the mechanical resonance frequency determined by the speed of sound in the direction of vibration. However, because the derivation is general, the specific vibration distribution in question will not need to be explicitly handled in the derivation because they have been solved in the general case in Eq. (5).

2.1 Short circuit analysis of the force factor

The constitutive equation describing the electric displacement of a piezoelectric k_{31} resonator is [15]

$$D_3(t) = d_{31}X_1 + \varepsilon_{33}^X \varepsilon_0 E_3(t). \quad (6)$$

By using the electromechanical coupling factor, this equation can be rewritten as

$$D_3(t) = e_{31}^* \frac{\partial u}{\partial x} + \varepsilon_{33}^{x_1} \varepsilon_0 E_3(t), \quad (7)$$

where e_{31}^* is the effective piezoelectric stress coefficient defined as $e_{31}^* = d_{31}/s_{11}^E$ and $\varepsilon_{33}^{x_1}$ is the relative permittivity having clamping in the length (1-direction). The actual piezoelectric stress coefficient e_{31} (non-star) is defined from clamped boundary conditions in the 2-direction and the 3-direction, whereas for the k_{31} resonator these boundaries are stress free. Thus, the effective piezoelectric stress coefficient is used as defined above. For the electrical boundary condition of zero electric potential case (short circuit), the external field is equal to zero. Therefore,

$$D_3(t) = e_{31}^* \frac{\partial u}{\partial x}, \quad (8)$$

and

$$\dot{D}_3 = e_{31}^* \frac{\partial^2 u}{\partial x \partial t}. \quad (9)$$

The current can be written as

$$i(t) = \int_{A_e} \dot{D}_3 dA_e, \quad (10)$$

where

$$dA_e = b dx. \quad (11)$$

Therefore,

$$i(t) = b \int_{-L/2}^{L/2} \dot{D}_3 dx. \quad (12)$$

Assuming that the sample is undergoing free vibration at the resonance frequency (constant E/short circuit conditions), we can apply Eq. (3) such that the current can be written as

$$i_0 = -2e_{31}^* u_0 b \omega_A. \quad (13)$$

This equation can also be written in terms of vibration velocity at the plate edge ($x = \pm L/2$), given $\omega u_0 = v_0$ for sinusoidal time varying displacement

$$i_0 = -2e_{31}^* b v_0. \quad (14)$$

The force factor A_{31} , defined as the ratio between short circuit current and edge vibration velocity, can then be written as

$$A_{31} = \frac{i_0}{v_0} = -2e_{31}^* b = -2b \frac{d_{31}}{s_{11}^E}. \quad (15)$$

2.2 Open circuit analysis of the voltage factor

For open circuit conditions the total electric displacement is equal to zero

$$\int_{-L/2}^{L/2} D_3(t) dx_1 = 0. \quad (16)$$

Therefore, the constitutive equation described in Eq. (7) can be written as

$$\int_{-L/2}^{L/2} D_3(t) dx_1 = \int_{-L/2}^{L/2} \left(e_{31}^* \frac{\partial u}{\partial x} + \varepsilon_{33}^{x_1} \varepsilon_0 E_3(t) \right) dx_1. \quad (17)$$

Assuming the variation of strain in thickness is negligible, the electric field across the thickness is uniform. Therefore, the $E_3(x, t) = -V(t)/a$. Integrating across the length of the resonator,

$$\int_{-L/2}^{L/2} E_3(x, t) dx = - \int_{-L/2}^{L/2} V(t)/a dx = \frac{e_{31}^*}{\varepsilon_{33}^{x_1} \varepsilon_0} \int_{-L/2}^{L/2} \frac{\partial u}{\partial x} dx. \quad (18)$$

This equation can be rewritten using Eq. (3) assuming natural vibration at the antiresonance frequency in open circuit conditions

$$LV_0/a = \frac{e_{31}^*}{\varepsilon_{33}^{x_1} \varepsilon_0} 2u_0. \quad (19)$$

Thus, the relationship between displacement and generated open circuit voltage for a k_{31} resonator in its antiresonance mode can be written as

$$V_0 = \frac{2ae_{31}^*}{L\varepsilon_{33}^{x_1} \varepsilon_0} u_0, \quad (20)$$

and the voltage factor (B_{31}), the ratio between open circuit voltage and edge displacement, can be written as

$$B_{31} = \frac{V_0}{u_0} = \frac{2a}{L} \frac{e_{31}^*}{\varepsilon_{33}^{x_1} \varepsilon_0} = \frac{2a}{L} \frac{g_{31}}{s_{11}^D} = \frac{2a}{L} h_{31}^*, \quad (21)$$

given negligible cross coupling. The effective piezoelectric stiffness coefficient h_{31}^* the electric field generated in the 3 direction (polarization direction) for an applied strain in the 1 direction under constant D conditions (open circuit) having free boundary conditions in the 2-direction and the 3-direction:

$$E_3 = h_{31}^* \frac{\partial u_1}{\partial x_1}, \quad (22)$$

the relationship between stress and strain under constant D

$$x_1 = s_{11}^D X_1, \quad (23)$$

and the relationship between generated electric field under constant D and stress X is

$$E_3 = g_{31} X_1. \quad (24)$$

2.3 Analysis of elastic compliance, piezoelectric charge coefficient, and the electromechanical coupling factor

It is well known that the sound velocity in a k_{31} resonator propagating in the 1-direction occurs is governed by the density and the elastic compliance under constant electric field [15]. The first resonance frequency in the k_{31} resonator corresponds to the s_{11}^E according to the equation

$$s_{11}^E = 1/((2Lf_A)^2 \rho). \quad (25)$$

By utilizing the measurement of the force factor, the piezoelectric charge coefficient can be computed

$$d_{31} = -A_{31}s_{11}^E/2b. \quad (26)$$

A more common approach to calculate this coefficient, frequently used in electrical resonance spectroscopy, is as follows: the off-resonance permittivity and resonance elastic compliance can be used to separate the piezoelectric charge coefficient from the coupling coefficient. k_{31} is calculated from a trigonometric function whose variables are the resonance and antiresonance frequencies [15]. Therefore, d_{31} can be expressed as

$$d_{31} = -k_{31}\sqrt{s_{11}^E\varepsilon_{33}^X\varepsilon_0}. \quad (27)$$

This approach assumes that the ε_{33}^X does not change in resonance conditions. The calculation of d_{31} using the force factor does not make this assumption, so it is expected to be more accurate. A detailed experimental analysis will follow in the next section.

By using the piezoelectric stress coefficient calculated at resonance (from the force factor) and the converse piezoelectric constant calculated at antiresonance (from the newly derived voltage factor), the clamped permittivity can be calculated in resonance conditions directly. Then, ε_{33}^X can be calculated using the k_{31}^2 .

$$\varepsilon_0\varepsilon_{33}^X(1 - k_{31}^2) = \varepsilon_0\varepsilon_{33}^{x_1} = \frac{e_{31}^*}{h_{31}^*} = \frac{A_{31}}{B_{31}} \frac{a}{Lb} \quad (28)$$

Permittivity has never been calculated directly in resonance conditions according to the authors' knowledge. Takahashi et al. has reported permittivity in resonance conditions, but assumes that only the motional capacitance changes and the clamped capacitance in resonance does not change. The validity of this assumption will be evaluated from the data in the next section.

3 Excitation of resonance and antiresonance using burst drive

In the burst mode experiment, the sample is first driven with an oscillating voltage in order to build up vibration. Then, the driving signal is removed, and thus the sample vibration decays at the system's natural frequency. Fig. 4a demonstrates the application of the burst mode using resonance methods (constant E). The sample is driven at its resonance frequency for a set number of cycles, after which a short circuit condition is imposed, inducing natural vibration at the electrical resonance frequency. Fig. 4b demonstrates the case where an open circuit condition is imposed, generating antiresonance vibration. For the open circuit condition, a bias voltage (not shown) can be generated along with the decaying oscillating voltage as reported by Chang [11]. This bias voltage is generated from the charge on the electrode at the time of introducing the open circuit condition. Depending on

the instantaneous charge before the open circuit condition is imposed, the bias voltage can be positive, negative, or zero. By driving the sample near the antiresonance frequency before the open circuit is introduced, the resulting bias voltage is greatly reduced because of the small current in this condition. This was the unique approach taken in this research for measuring the antiresonance burst response.

By applying the burst mode at resonance (short circuit) and antiresonance (open circuit) conditions, the loss factors and the real properties of the material can be measured. For a damped linear system oscillating at its natural frequency, the quality factor can be described using the relative rate of decay of vibration amplitude. In general, [3]

$$Q = \frac{2\pi f}{2 \ln(v_1/v_2)/(t_2 - t_1)}. \quad (29)$$

This equation is true at both resonance and antiresonance. At resonance, the current is proportional to the vibration velocity; therefore, its decay can be used. Similarly, the voltage decay can be used at antiresonance to determine the quality factor at antiresonance.

4 Experimental application

4.1 Sample selection

The burst mode experiment was performed on k_{31} samples of commercially available PZT compositions: three PIC 184 (PI Ceramic, Germany) k_{31} samples and three PIC 144 (PI Ceramic, Germany) k_{31} samples, whose low power properties are listed in Tab. 1. All the samples have a geometry of $40 \times 6 \times 1 \text{ mm}^3$. Commercially available materials were chosen because they provide the most relevant results from a practical perspective. The samples were supported from the center (nodal point) by adjustable spring loaded electrodes. Each sample in each condition (resonance and antiresonance) was measured twice. After every measurement, the sample was removed, turned over, and reloaded into the sample holder. Therefore, each data point presented is an average of six measurements and the error bars are the standard deviation of these measurements. Previous researchers either did not present multiple measurements or did not discuss the effect of reloading the sample on the standard deviation [3, 5, ?]. By measuring one sample several times without removing and reloading it, the standard deviation is significantly reduced, but the true value of the material property remains more ambiguous. Therefore, the fact that the samples were removed and reloaded in the sample holder is highlighted. The measurement of the properties of piezoelectric material having low losses, such as hard PZT, are more sensitive to the sample holder positioning.

4.2 Experimental setup and procedure

The experimental setup diagram can be seen in Fig. 5. The sample was driven by a function generator (Siglent SDO342) through a power amplifier (NF4010). The sample was held at the nodal point. The drive period was set at 10 cycles. For the short circuit measurement, the sample was driven at its resonance frequency at 50V/mm using the burst mode of the function generator. After the burst signal finished, the applied voltage to the sample was 0V, which is equivalent to a short circuit condition. The current and vibration then decayed. The measured voltage during the short circuit condition indicated an added effective inductive load on the order of 1Ω . This was due to the current flow through the BNC cable from the amplifier. After applying the burst signal, antiresonance vibration was induced by isolating the sample from the driving signal using an electromechanical relay. The electromechanical relay was triggered with a precise time delay from the burst signal using the second channel of the function generator.

For the open circuit experiments, the sample was driven close to its antiresonance frequency (minimum current), and for the short circuit experiments, the sample was driven close to its resonance frequency (maximum current). This is because after imposing the open circuit or short condition, the sample's oscillating frequency immediately shifts to the frequency particular to the electrical boundary condition, antiresonance or resonance, respectively. If this frequency shift is significant, transient higher harmonics are generated and they cause the vibration decay to become irregular and difficult to analyze. By driving the system at its resonance frequency prior to applying the short circuit and the antiresonance frequency prior to applying open circuit, transient higher harmonics were minimized and random error was reduced significantly.

The current was measured by a 10x wire loop and a current probe (Tektronix TCPA300 w/ TCP 305 probe). The current probe was verified to produce accurate readings for the current levels tested by measuring the current produced in a $1k\Omega$ precision resistor near the experimental resonance frequency.

For the open circuit experiments, a electromechanical relay was used to isolate the sample from the signal. The function generator used has two channels, allowing for a programmable delay between them. One of the channels was responsible for providing the burst signal (10 sinusoidal cycles) through the amplifier, and the other channel was responsible for driving the relay directly. The channel powering the relay was normally on at 10V, and it decreased to 0V after the trigger was initiated. The delay for the turn off time of the relay was approximately 0.45ms. This delay time was added to the burst signal channel along with the delay time needed to allow for the 10 drive cycles to the sample to build up vibration. The open circuit voltage was measured using a 100x voltage probe (Tektronix P1500). The voltage probe had a resistance of $10M\Omega$, much higher than the antiresonance impedance of the samples, and the capacitance of the probe was more than a thousand times less than that of the samples measured.

Additional measurement issues should be taken into consideration when selecting the sample geometry, in

addition to isolating the vibration mode of analysis. A sufficient width for the sample should be chosen to generate the level of current needed according to the force factor for the equipment to make accurate measurements. Similarly, for antiresonance, the a/L ratio changes the voltage factor. Usually, voltage can be measured with high accuracy using an oscilloscope without special considerations. Depending on the thickness and length, over a 400V can be generated, as reported by Uchino [1], so therefore the a/L ratio may need to be considered for the sample fabrication in order to avoid voltage levels which may damage measurement equipment.

4.3 Data collection method

A crucial factor in the attainment of repeatable and accurate results was the data collection and analysis method used, and the storage capacity of the oscilloscope. A LabVIEW program utilizing a function which estimates the frequency and amplitude of the dominant harmonic signal from a Fourier transform analysis was applied. It was found that the built-in FFT analysis function of the oscilloscope lacks sufficient resolution, both in frequency and amplitude measurements, to provide systematic results; analyzing the waveforms on the PC provided better final results. Small instability in the signal can cause large error in frequency measured from zero crossing of the oscillating signals and amplitude characterization using maximum values. Therefore, a FFT analysis is the most appropriate. The name of the LabVIEW function used to accomplish this was called “Extract Single Tone,” by which the frequency and amplitude of the signal were measured by interpolating the FFT spectrum of the waveform. The oscilloscope time base was initially set to be large enough to allow the vibration velocity to decrease ten times from the maximum value within a single capture of the oscilloscope. After this acquisition, a smaller time base was used to approximate the capture of data at specific instances in time. By moving the viewing window forward (with the small time base), data for different vibration levels could be measured. For the hard PZT measured in this study, the smaller time base used was 4 cycles, and for the semi-hard PZT the time base used was 2 cycles. A smaller number of cycles must be used for the semi-hard PZT because its vibration signal decays more rapidly. The initial use of the large time base for the waveform acquisition and then the subsequent decrease in the time base showed no apparent difference in measurement from using a small time base for the initial acquisition. The ability of the FFT function used over several cycles increased the measurement integrity significantly over using the peak values of the waveforms to determine signal amplitude, decay, and frequency.

5 Results and discussion

5.1 Measurement of the force factor and voltage factor

Regarding resonance characterization, the ratio between the short circuit current and edge vibration velocity was used to calculate the force factor and the piezoelectric stress constant, $e_{31}^* = d_{31}/s_{11}^E$, according to Eq. (14).

Using the resonance frequency, the compliance was calculated, and the piezoelectric charge coefficient as well using the piezoelectric stress coefficient. The resonance characterization for PIC 144 and PIC 184 is shown in Figs. 6a and 6b. PIC 144 shows lower property values (d_{31} , s_{11}^E , e_{31}^*) than PIC 184, which is expected because PIC 144 is a hard PZT composition and has a higher quality factor judging from its low power properties (Tab. 2). The properties d_{31} , s_{11}^E , and e_{31}^* of PIC 184 and PIC 144 change linearly with vibration velocity. However, PIC 144 has more stable properties with vibration velocity but a larger deviation from a linear change in material properties with vibration velocity. That being said, the change in properties of PIC 144 with respect to the low power properties (lowest vibration level) is significantly less than that of PIC 184.

By utilizing the displacement and open circuit voltage at antiresonance, the voltage factor B_{31} and the effective piezoelectric stiffness coefficient h_{31}^* were calculated using Eq. (20) (Fig. 7). The coupling factor was calculated using the resonance and antiresonance frequencies, and the trigonometric function defined for the k_{31} resonator [15]. The coupling factor increases with the vibration velocity; the change in the coupling factor with vibration velocity (slope) of PIC 184 is three times larger than that of PIC 144. h_{31}^* decreases with increasing vibration velocity, contrary to the trend of the other properties. That being said, it has a much smaller dependence on vibration velocity than the other properties, namely those determined at resonance.

5.2 Characterization of losses at resonance and antiresonance

Using the decay of vibration at resonance and antiresonance, the quality factors were calculated. Each data point used amplitude data from two vibration measurements; therefore, the scale was readjusted as an average of the vibration velocity. Fig. 8 shows the results; a log-log plot was used to easily distinguish and compare the trends between the two compositions. PIC 144 shows stable characteristics of the quality factor, until about 150 mm/s RMS, after which a sharp degradation in the quality factors occurred. PIC 184, however, showed an immediate decrease in its quality factors. Q_B was larger than Q_A for both the materials.

5.3 Characterization of permittivity ε_{33}^X in high power resonance conditions

5.3.1 Off resonance approximation of the permittivity

Traditionally, the dielectric permittivity is measured by applying an oscillating electric potential at an off-resonance frequency and measuring the resulting charge or current [15]. The dielectric permittivity has not been measured at resonance high power conditions because the dielectric response in this condition does not display a distinct characteristic which can be measured to compute it. Therefore, researchers have used one of the two approaches to estimate the permittivity in high power conditions:

1. Assume the permittivity measured in off-resonance conditions applies to resonance conditions. This approach is problematic because the stress conditions and the frequency is different at resonance, and therefore

the property is expected to change, similar to other properties.

2. The other approach is to assume that the permittivity in high power conditions can be considered as a perturbation of the off-resonance permittivity using a variation in the motional capacitance, which is proportional to d_{31}^2/s_{11}^E for the k_{31} mode.

The first approach is flawed because the elastic and piezoelectric properties of the material are known to change with applied stress; therefore, the dielectric response must also follow a similar tendency because s^E , d , and ε^X all have extrinsic contributions from non-180° domain walls which are strongly affected by applied stress. Researchers using the second approach assume that clamped permittivity ε^x of the material is the same in high power resonance conditions and in low power off-resonance conditions. The permittivity under constant stress (ε_{33}^X) is a combination of the motional and clamped dielectric response of the material. Assuming ε^x from off-resonance measurements, adjusting the motional contribution to ε^X according the piezoelectric charge constant, the compliance can determine the permittivity ε^X in these conditions. The basis for the assumption of the equivalency of the lower power and high power clamped permittivity is as follows:

The dielectric permittivity ε in PZT thin films are much lower than the permittivity ε^X in bulk PZT. This is because the substrate effectively clamps the PZT film, and thereby significantly reduces the non-180° domain wall motion and its contribution to the permittivity. The 180° domain wall motion contribution to the permittivity, however, is relatively undisturbed because it does not result in change in strain and therefore is relatively unaffected by the substrate [16]. In the k_{31} resonator examined, ε^x refers to the dielectric response of the material with an applied field in the 3-direction and polarization in the 3-direction with clamping in the 1-direction. This clamping results is far less clamping than the substrate clamping in PZT thin films. Because the effective stresses applied due to resonance vibration of the k_{31} resonator are in the 1-direction, and the ε^x represents the permittivity after “clamping out” the domain wall contributing to domain wall motion the 1-direction, the following equality should be true: $\varepsilon_{low\ power}^x = \varepsilon_{high\ power}^x$.

This was the approach taken by Takahashi et. al. They have reported permittivity in resonance conditions, but assume that only the motional capacitance changes and the clamped capacitance in resonance does not [4]. For the burst method, they have reported the motional capacitance (d_{31}^2/s_{11}^E) to remain constant, and therefore the permittivity, which is calculated partially from off-resonance measurements, to be constant as well.

That being said, there may exist other phenomena which also affect the clamped permittivity. This may include the frequency response. The clamped permittivity may change with increasing frequency due to the dependence of domain wall motion spectral response. Therefore, this assumption may be invalid for this or other reasons, and it is preferred to calculate the permittivity using only data from resonance measurements in order to ensure compatibility between measurements to resolve a final property.

5.3.2 Determination of the permittivity using the voltage factor and force factor in resonance conditions

By using the piezoelectric stress coefficient calculated at resonance (from the force factor) and the converse piezoelectric constant calculated at antiresonance (from the newly derived voltage factor), the clamped permittivity can be calculated in resonance conditions directly. Then from Eq. 30 ε_{33}^X can be calculated using the k_{31}^2 :

$$\varepsilon_0 \varepsilon_{33}^X (1 - k_{31}^2) = \varepsilon_0 \varepsilon_{33}^{x_1} = \frac{e_{31}^*}{h_{31}^*} = \frac{A_{31}}{B_{31}} \frac{a}{Lb}. \quad (30)$$

The change in permittivity with vibration velocity can be seen on Fig. 9. The off-resonance permittivity measured for the samples is in good agreement with the low vibration velocity permittivity measured through the burst technique as seen in this figure. The off-resonance permittivity is represented by a star symbol. The clamped and free permittivity are both changing with increasing vibration velocity. The permittivity of PIC 184 is larger than that of PIC 144, and this is to be expected because PIC 184 is a semi-hard PZT with larger off-resonance permittivity. From the low vibration state to the high one, the permittivity of both compositions increase. However, the increase in PIC 184 is larger, demonstrating that its properties have a larger dependence on vibration conditions.

As mentioned earlier in this section, we expect $\varepsilon_{low\ power}^x = \varepsilon_{high\ power}^x$ because of the clamping out of non-180° domain walls. However, the result shown in this study demonstrates that a majority of the change seen in the free permittivity can actually be attributed to the clamped permittivity change. The open circuit voltage generated during antiresonance may have caused the property changes being reported in this study. For the PIC 184 samples, the largest voltage generated was 85V/mm RMS @ 450mm/s RMS, and for the PIC 144 samples the largest voltage was 120V/mm RMS @ 600mm/s RMS. The open circuit voltage generated may cause domain reorientation in the 180° domain wall regions. The motional capacitance (proportional to the difference, $\varepsilon_{33}^X - \varepsilon_{33}^{x_1}$) remains fairly constant, so it cannot explain the change in permittivity.

The difference in the $\varepsilon_{low\ power}^x$ and $\varepsilon_{high\ power}^x$ may also be due to the details of the clamping applied. As mentioned earlier, in the k_{31} resonator examined, the clamping considered is the 1-direction only. Therefore, it should not be expected that all of non-180° domain walls are clamped because the clamping is dissimilar from the substrate clamping effect seen in thin films. From the data in Fig. 9, it can be said that the change in clamped permittivity represents the stresses in the 1-direction affects non-180° domain wall motion in the 2 and 3 direction.

6 Summary

Traditionally, characterization of piezoelectric materials in resonance is accomplished using continuous drive methods with impedance spectroscopy. However, the burst/transient method can be used instead. It affords simple experimental application, reasonable application of linear theories, and naturally lends itself toward high power measurements. In this chapter, a comprehensive measurement approach toward characterization of the k_{31}

resonator was demonstrated using resonance and antiresonance drive methods. The experimental procedure to achieve both of these conditions was described. The measurement incorporated the use of the force factor analysis to characterize the elastic compliance and piezoelectric charge coefficient as used by other researchers. Antiresonance analysis using the voltage factor was performed for the first time. In antiresonance, the ratio between open circuit voltage and displacement gives the voltage factor, which is proportional to the converse piezoelectric coefficient. With increasing vibration level, the elastic compliance (constant electric field), piezoelectric charge constant, and piezoelectric stress constant increased. At the same time, the converse piezoelectric constant and the quality factors decreased. Also, the calculation of the permittivity in resonance conditions only using measurements from resonance conditions was demonstrated. The results show that the change in the clamped and free permittivity for the k_{31} resonators tested were of similar levels; therefore, the change in motional capacitance was small and change in clamped capacitance dominated the dependence of ε_{33}^X on vibration level.

Acknowledgment

The authors would also like to acknowledge the Office of Naval Research for sponsoring this research under grant number: ONR N00014-12-1-1044.

References

- [1] K. Uchino, Y. Zhuang, and S. O. Ural, "Loss determination methodology for a piezoelectric ceramic: new phenomenological theory and experimental proposals," *Journal of Advanced Dielectrics*. **01**, 10 (2011).
- [2] E. Hennig, E. Wehrsdorfer, S. Lürtzing, B. Kolle, and W. Plötner, "Large signal characterization of hard PZT materials," *Journal of the European Ceramic Society*. **25**, 12 (2005).
- [3] M. Umeda, K. Nakamura, and S. Ueha, "The measurement of high-power characteristics for a piezoelectric transducer based on the electrical transient response," *Japanese Journal of Applied Physics*. **37**, 5322 (1998).
- [4] S. Takahashi, Y. Sasaki, M. Umeda, K. Nakamura, and S. Ueha, "Characteristics of piezoelectric ceramics at high vibration levels," *MRS Proceedings*. **604**, 15 (1999).
- [5] M. Umeda, K. Nakamura, and S. Ueha, "Effects of vibration stress and temperature on the characteristics of piezoelectric ceramics under high vibration amplitude levels measured by electrical transient responses," *Japanese Journal of Applied Physics*. **38**, 5581 (1999).
- [6] T. Tou, Y. Hamaguti, Y. Maida, H. Yamamori, K. Takahashi, and Y. Terashima, "Properties of $\text{Bi}_{0.5}\text{Na}_{0.5}\text{TiO}_3\text{BaTiO}_3(\text{Bi}_{0.5}\text{Na}_{0.5})(\text{Mn}_{1/3}\text{Nb}_{2/3})\text{O}_3$ lead-free piezoelectric ceramics and its application to ultrasonic cleaner," *Japanese Journal of Applied Physics*. **48**, 07GM03 (2009).

- [7] H. Nagata, Y. Hiruma, and T. Takenaka, "High power piezoelectric characteristics for perovskite-type lead-free ferroelectric ceramics," *Integrated Ferroelectrics*. **115**, 63 (2010).
- [8] M. Hagiwara, S. Takahashi, T. Hoshina, H. Takeda, and T. Tsurumi, "Analysis of nonlinear transient responses of piezoelectric resonators," *IEEE Transactions on Ultrasonics, Ferroelectrics, and Frequency Control*. **58**, 1721 (2011).
- [9] Y. Noumura, Y. Hiruma, H. Nagata, and T. Takenaka, "High-power piezoelectric characteristics of $\text{Bi}_4\text{Ti}_3\text{O}_{12}\text{SrBi}_4\text{Ti}_4\text{O}_{15}$ -based ferroelectric ceramics," *Japanese Journal of Applied Physics*. **49**, 09MD02 (2010).
- [10] Y. Hiruma, T. Watanabe, H. Nagata, and T. Takenaka, "Piezoelectric properties of $(\text{Bi}_{1/2}\text{Na})\text{TiO}_3$ -based solid solution for lead-free high-power applications," *Japanese Journal of Applied Physics*. **47**, 7659 (2008).
- [11] K. Chang and M. Ouyang, "Open-circuit test of a PZT vibrator and its applications," *Ultrasonics*. **41**, 15 (2003).
- [12] K. Chang, "Electrical characteristics of a piezoelectric vibrator in open-circuit transient state," *Japanese Journal of Applied Physics*. **43**, 7604 (2004).
- [13] K. Chang, "Investigation of electrical transient behavior of an ultrasonic transducer under impulsive mechanical excitation," *Sensors and Actuators A: Physical*. **133**, 407 (2007).
- [14] S. O. Ural, "High Power Piezoelectric Characterization for Piezoelectric Transformer Development," PhD thesis, The Pennsylvania State University, 2010.
- [15] T. Ikeda, *Fundamentals of Piezoelectricity*. (Oxford University Press, New York, 1996).
- [16] F. Xu, S. Trolier-McKinstry, W. Ren, B. Xu, Z.L. Xie, and K.J. Hemker, "Domain wall motion and its contribution to the dielectric and piezoelectric properties of lead zirconate titanate films," *Journal of Applied Physics*, **89**, 1336 (2001).

Figures

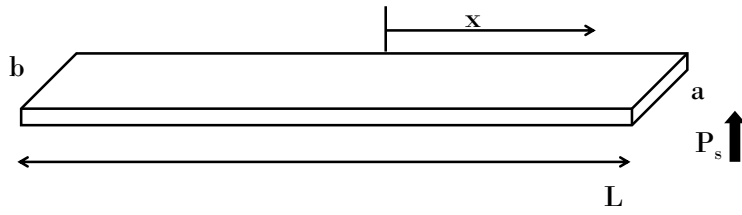


Figure 1 Geometry of a k_{31} resonator

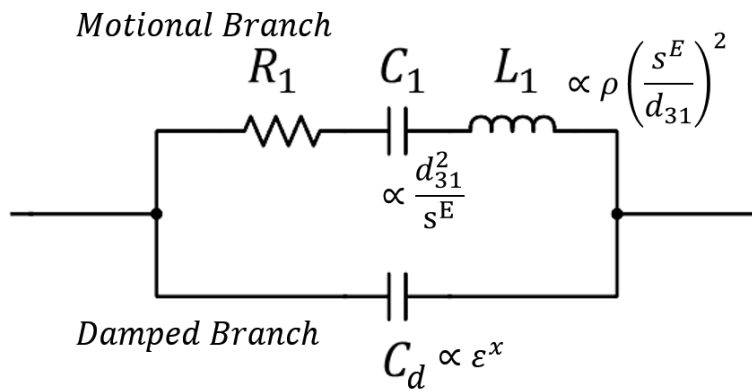


Figure 2 Simplified equivalent circuit of a k_{31} piezoelectric resonator (material property equivalencies are presented for illustration)

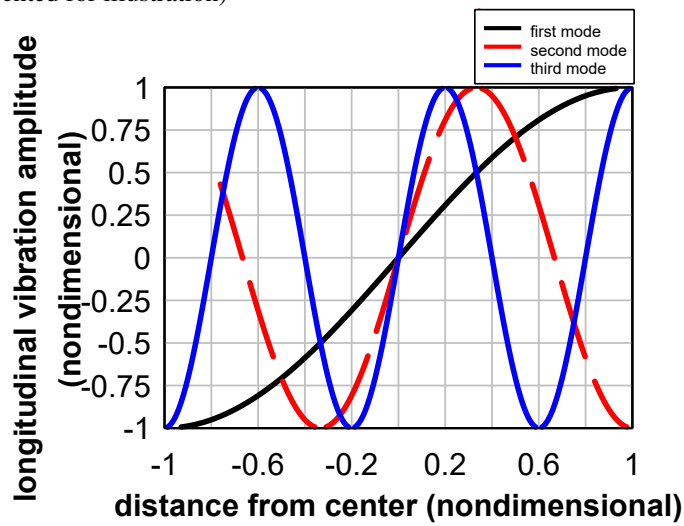


Figure 3 Displacement distribution for the first three resonance modes for the k_{31} resonator

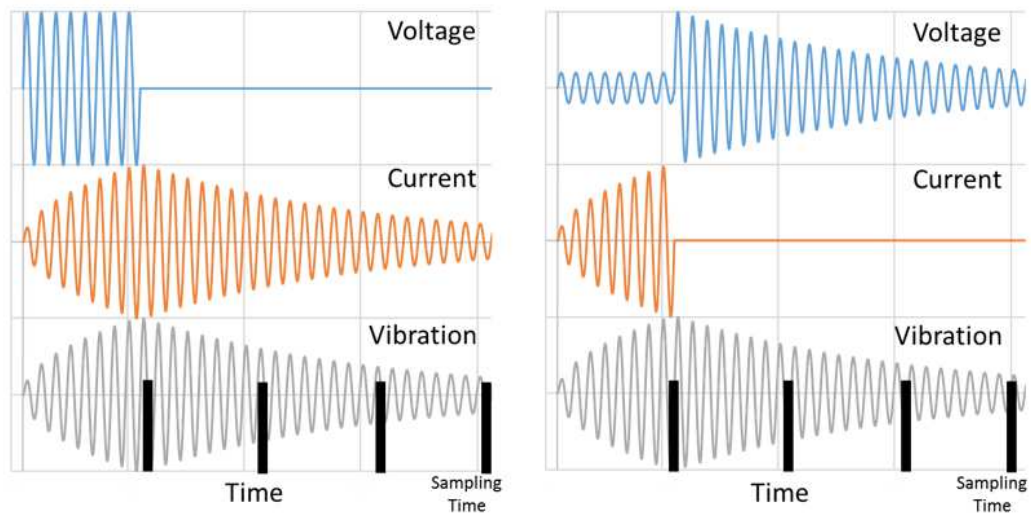


Figure 4 Qualitative waveforms describing voltage, current, and vibration (a) before and after short circuit and (b) before and after open circuit

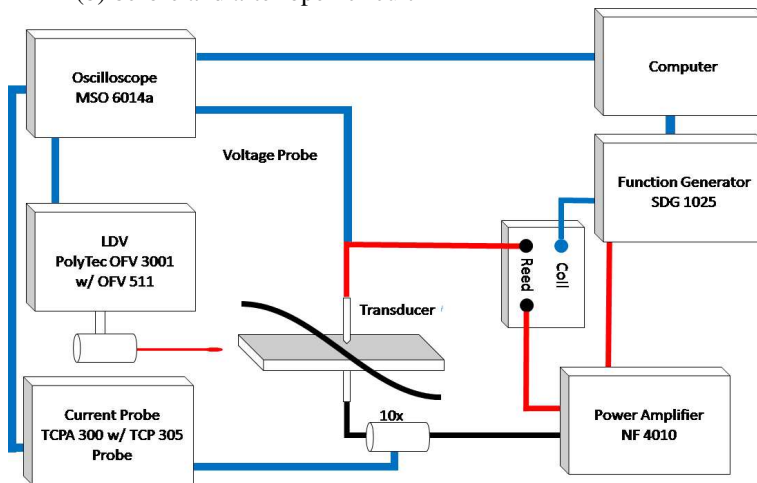


Figure 5 Experimental setup to apply burst method measurement

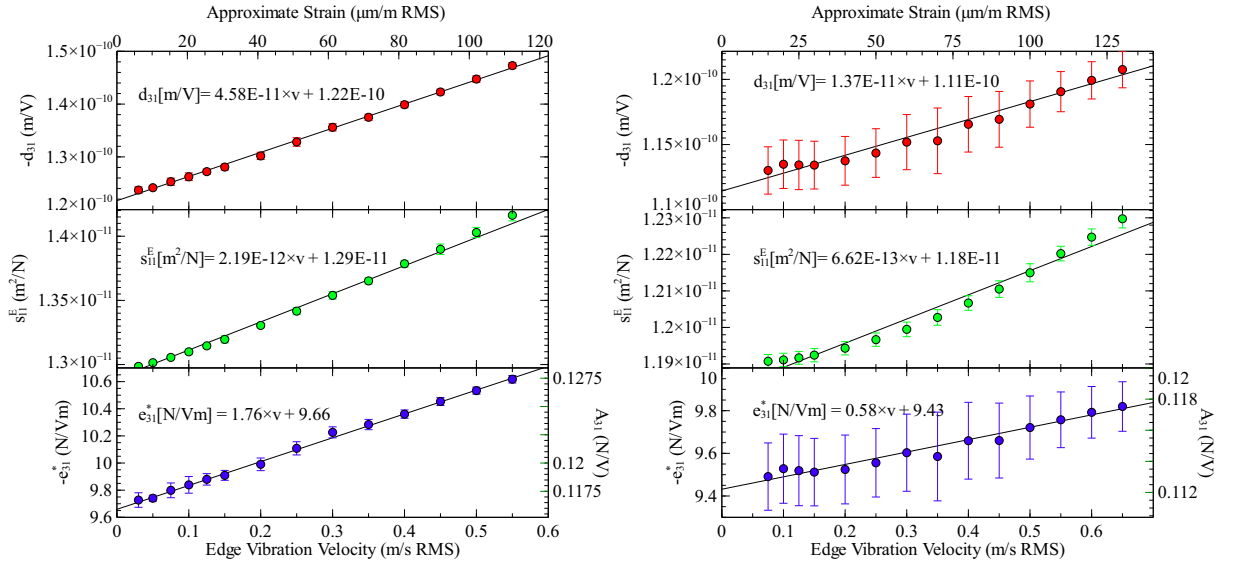


Figure 6 (a) Resonance characterization of PIC 184 k_{31} and (b) resonance characterization of PIC 144 k_{31}

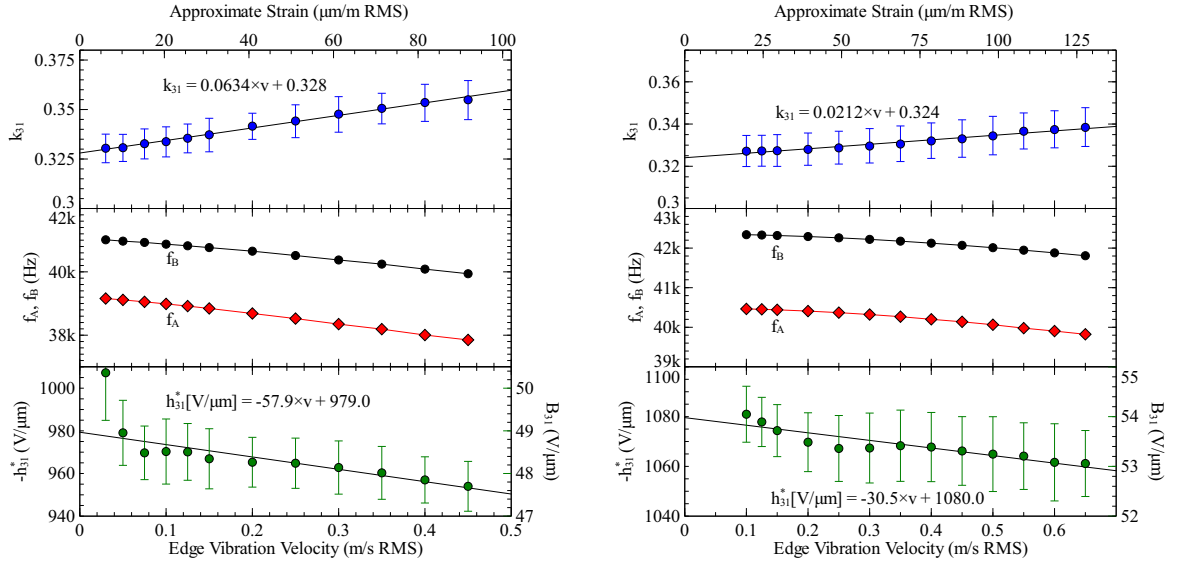


Figure 7 (a) Antiresonance characterization of PIC 184 k_{31} and (b) antiresonance characterization of PIC 144

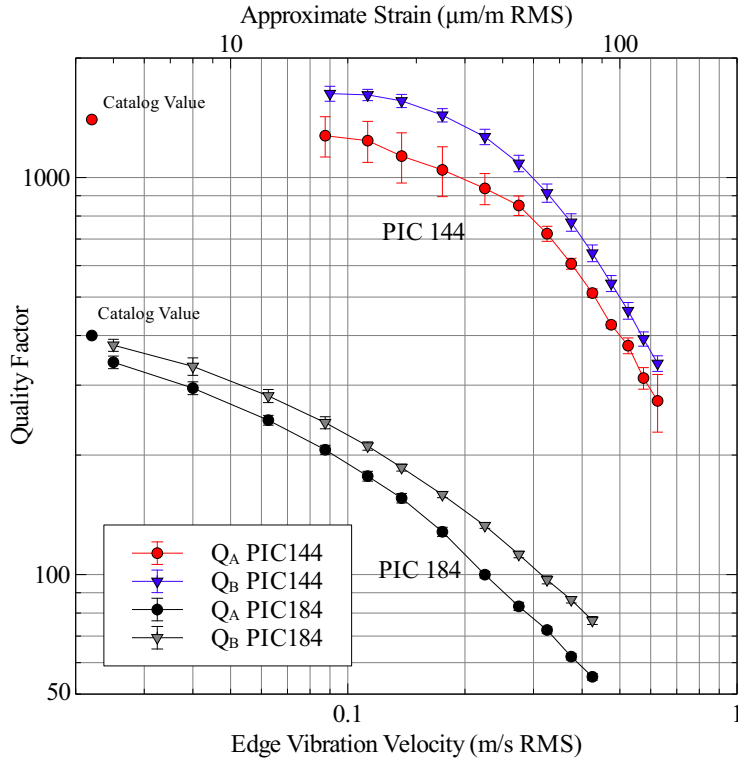


Figure 8 Change in quality factors with vibration velocity for PIC 184 and PIC 144 k_{31} samples

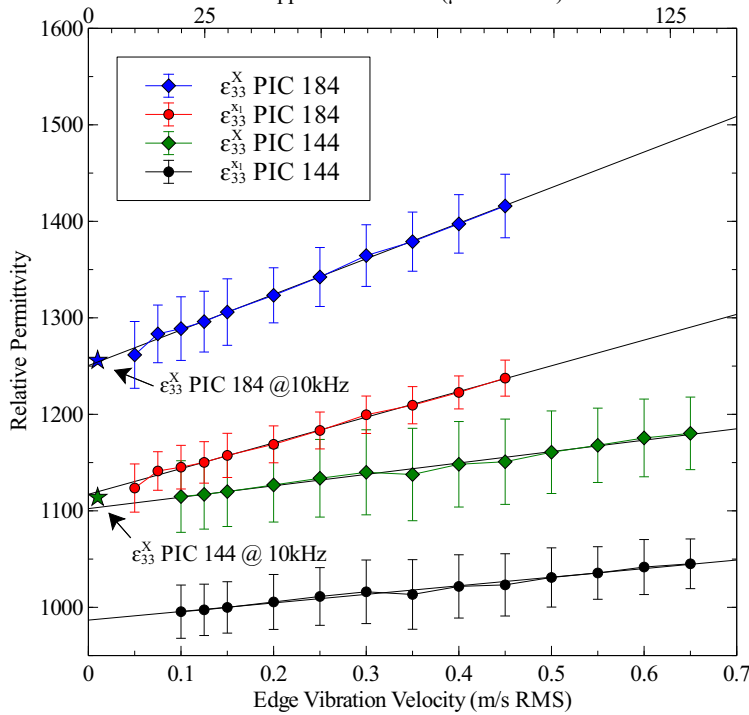


Figure 9 Change in dielectric permittivity with increasing vibration velocity

Tables

Symbol	Description	Unit
D_3	electric displacement	C/m ²
E_3	electric field	V/m
$\partial u / \partial x$	strain	-
e_{31}^*	transverse piezoelectric stress constant	N/Vm
s_{11}^E	elastic compliance under constant electric field	m ² /N
d_{31}	transverse piezoelectric charge constant	m/V
$\varepsilon_{33}^{x_1}$	permittivity under constant strain/clamped in the 1-direction	-
ε_{33}^X	relative permittivity under free stress conditions	-
ε_0	permittivity of free space	F/m
$u(x, t)$	spatial displacement distribution	m
t	time	s
A_e	area of the electrode	m ²
$i(t)$	current	A
i_0	current amplitude	A
ω	angular frequency	rad/s
x	position along the length (1-direction)	m
u_0	edge displacement amplitude	m
$v(x, t)$	spatial vibration velocity distribution	m/s
v_0	edge vibration velocity amplitude	m/s

Table 1: Description of symbols

	$\varepsilon_{33}^X @ 10\text{kHz}$	$s_{11}^E (\text{m}^2/\text{N})$	$-d_{31} (\text{m/V})$	k_{31}	$\tan \delta' @ 10\text{kHz}$	Q_m
PIC 184	1260	1.30E-11	124E-12	0.330	0.004	340
PIC 144	1110	1.19E-11	113E-12	0.327	0.0015	1300

Table 2: Low power properties of PIC 184 and PIC 144 as calculated from the burst mode